The Astrophysical Journal, 779:7 (17pp), 2013 December 10 doi:10.1088/0004-637X/779/1/7

DWARF SPHEROIDAL SATELLITES OF M31. I. VARIABLE STARS AND STELLAR POPULATIONS IN ANDROMEDA XIX*

Felice Cusano[1], Gisella Clementini[1], Alessia Garofalo[1,2], Michele Cignoni[2], Luciana Federici[1], Marcella Marconi[3], Ilaria Musella[3], Vincenzo Ripepi[3], Konstantina Boutsia[4], Marco Fumana[5], Stefano Gallozzi[4], and Vincenzo Testa[4]
[1] INAF-Osservatorio Astronomico di Bologna, Via Ranzani 1, I-40127 Bologna, Italy; felice.cusano@oabo.inaf.it, gisella.clementini@oabo.inaf.it, luciana.federici@oabo.inaf.it
[2] Dipartimento di Astronomia, Università di Bologna, Via Ranzani 1, I-40127 Bologna, Italy; alessia.garofalo@studio.unibo.it, michele.cignoni@unibo.it
[3] INAF-Osservatorio Astronomico di Capodimonte, Salita Moiariello 16, I-80131 Napoli, Italy; marcella@na.astro.it, ilaria@na.astro.it, ripepi@na.astro.it
[4] INAF-Osservatorio Astronomico di Roma, Via di Frascati 33, I-00040 Monte Porzio Catone, Italy; konstantina.boutsia@oa-roma.inaf.it, stefano.gallozzi@oa-roma.inaf.it, vincenzo.testa@oa-roma.inaf.it
[5] INAF-IASF Milano, Via E. Bassini 15, I-20133 Milano, Italy; fumana@lambrate.inaf.it
Received 2013 August 11; accepted 2013 October 4; published 2013 November 15

ABSTRACT

We present B, V time-series photometry of Andromeda XIX (And XIX), the most extended (half-light radius of 6.′2) of Andromeda's dwarf spheroidal companions, which we observed with the Large Binocular Cameras at the Large Binocular Telescope. We surveyed a $23' \times 23'$ area centered on And XIX and present the deepest color–magnitude diagram (CMD) ever obtained for this galaxy, reaching, at $V \sim 26.3$ mag, about one magnitude below the horizontal branch (HB). The CMD shows a prominent and slightly widened red giant branch, along with a predominantly red HB, which extends to the blue to significantly populate the classical instability strip. We have identified 39 pulsating variable stars, of which 31 are of RR Lyrae type and 8 are Anomalous Cepheids (ACs). Twelve of the RR Lyrae variables and three of the ACs are located within And XIX's half light radius. The average period of the fundamental mode RR Lyrae stars ($\langle P_{ab} \rangle = 0.62$ days, $\sigma = 0.03$ days) and the period–amplitude diagram qualify And XIX as an Oosterhoff-Intermediate system. From the average luminosity of the RR Lyrae stars ($\langle V(\mathrm{RR}) \rangle = 25.34$ mag, $\sigma = 0.10$ mag), we determine a distance modulus of $(m - M)_0 = 24.52 \pm 0.23$ mag in a scale where the distance to the Large Magellanic Cloud (LMC) is 18.5 ± 0.1 mag. The ACs follow a well-defined Period–Wesenheit (PW) relation that appears to be in very good agreement with the PW relationship defined by the ACs in the LMC.

Key words: galaxies: dwarf – galaxies: individual (Andromeda XIX) – Local Group – stars: distances – stars: variables: general – techniques: photometric

Online-only material: color figures, machine-readable table

1. INTRODUCTION

The number of satellites known to surround the Andromeda spiral galaxy (M31) has increased dramatically in the last few years thanks to the systematic imaging of the M31 halo being carried out by the Pan-Andromeda Archaeological Survey (PAndAS; Martin et al. 2006, 2009; Ibata et al. 2007; Irwin et al. 2008; McConnachie et al. 2008, 2009; Richardson et al. 2011), the Sloan Digital Sky Survey (SDSS; Zucker et al. 2004, 2007; Slater et al. 2011; Bell et al. 2011), and, lately, the Panoramic Survey Telescope and Rapid Response System 1 survey (Pan-STARRS1; Martin et al. 2013). The latest census of the M31 companions currently counts 31 dwarf spheroidal galaxies (dSphs) whose luminosities range from 10^4 to $10^8 L_\odot$. This number is expected to grow as new diffuse stellar systems are being discovered in the M31 halo (e.g., PAndAS-48; Mackey et al. 2013) whose actual nature, whether extended globular clusters (GCs) or ultra-faint dwarfs (UFDs) like those discovered around the Milky Way (MW), remains to be established. In the framework of the hierarchic formation of structures, the dSph satellites we observe today around M31 may be the survivors of Andromeda's building process. Their stellar content can thus provide insight to reconstruct the star formation history (SFH) and the merging episodes that led to the early assembling of the M31 halo. The synthetic modeling of deep color–magnitude diagrams (CMDs) represents the most direct way for understanding the formation history of a galaxy. However, the CMDs currently available for the M31 dSphs generally sample only the brightest stars (e.g., Zucker et al. 2004; McConnachie et al. 2008; Richardson et al. 2011; Bell et al. 2011), and even when *Hubble Space Telescope* (*HST*) data are available (Pritzl et al. 2002, 2004, 2005; Mancone & Sarajedini 2008; Yang & Sarajedini 2012) they only reach slightly below the horizontal branch (HB), because observing the main sequence turn-off (MSTO) of the oldest stellar populations at the distance of M31 [$(m - M)_0 = 24.47 \pm 0.07$ mag, $D = 783$ kpc, McConnachie 2012, or $(m - M)_0 = 24.42 \pm 0.06$ mag, $D = 766$ kpc, Federici et al. 2012] requires of the order of tens of *HST* orbits.

The pulsating variable stars are a powerful alternative tool to investigate the different stellar generations occurred in the M31 dSphs, as Classical Cepheids can be used to trace the young stars (typical ages ranging from a few to a few hundred Myr) and the RR Lyrae stars, which are comparably old but about 3 mag brighter than the MSTO, can allow us to unravel the oldest stars born more than 10 Gyr ago. Using characteristics like the mean period of the fundamental-mode (RRab) and first-overtone (RRc) pulsators and the ratio of the number of RRc (N_c) to total number of RR Lyrae stars (N_{ab+c}) ($f_c = N_c/N_{ab+c}$), the MW field and cluster RR Lyrae are divided into two different groups (Oosterhoff 1939): Oosterhoff type I (Oo I) clusters have

* Based on data collected with Large Binocular Cameras at the Large Binocular Telescope.

$\langle P_{ab}\rangle \simeq 0.55$ d, $\langle P_c\rangle \simeq 0.32$ days, and $f_c \sim 0.17$; and Oosterhoff type II (Oo II) clusters have $\langle P_{ab}\rangle \simeq 0.65$ d, $\langle P_c\rangle \simeq 0.37$ days, and $f_c \sim 0.44$.

Different Oosterhoff types also imply slightly different ages and metallicities (van den Bergh 1993), as Oo II clusters are more metal-poor and older than Oo I systems. Recent studies (see, e.g., Catelan 2009, for a review) confirmed the Oosterhoff dichotomy to occur not only among the MW GCs, but also for field variable stars in the MW halo.

On the other hand, the separation in Oosterhoff groups seems to be a characteristic of the MW, since the dSphs around our galaxy, as well as their respective GCs, have $0.58 \leqslant \langle P_{ab}\rangle \leqslant 0.62$ days, and Oo-Intermediate (Oo-Int) properties (Catelan 2009; Clementini et al. 2010 and references therein). The characterization of the RR Lyrae population in M31 and in its companions is still at an early stage. In a deep survey of the M31 halo, Brown et al. (2004) identified 55 RR Lyrae stars (29 RRab, 25 RRc, and one double-mode, RRd, pulsator) in a $3\farcm5 \times 3\farcm7$ field along the southeast minor axis of the galaxy. Based on their pulsation properties, Brown et al. (2004) concluded that unlike in the MW, the old population in the M31 halo has Oo-Int properties. However, a different conclusion was reached by Sarajedini et al. (2009) who identified 681 RR Lyrae variables (555 RRab and 126 RRc) based on the *HST*/Advanced Camera for Surveys (ACS) observations of two fields near M32, at a projected distance between 4 and 6 kpc from the center of M31, and concluded that these M31 fields have Oo-I properties. A total of 108 RR Lyrae stars were identified by Jeffery et al. (2011) in six *HST*/ACS ultra-deep fields located in the disk, stream, and halo of M31, showing that the RR Lyrae population appears mostly to be of the Oo-I and Oo-Int types. Of the M31 globular clusters only two had the RR Lyrae stars fully characterized: B514 was found to have Oo-Int properties (Clementini et al. 2009) and G11 to be an Oo II GC (Contreras Ramos et al. 2013). Six of the M31 dSphs have been analyzed so far for variability and RR Lyrae stars have been identified in all of them (Pritzl et al. 2002, 2004, 2005; Mancone & Sarajedini 2008; Yang & Sarajedini 2012). According to these studies, all three Oosterhoff types (Oo I, Oo II, and Oo-Int) seem to be present among the M31 satellites. These previous studies of variables in the M31 dSphs are based on the Wide Field Planetary Camera 2 onboard the *HST* data. However, the HB of the M31 satellites can easily be reached from the ground with 8–10 m class telescopes. The ground-based facilities usually allow for coverage of areas significantly larger than the half-light radius (r_h) of the M31 satellites, which are often rather extended, thus attaining more complete and statistically significant samples. We have obtained multi-band photometry of a sample of the M31 dSph satellites (see Clementini et al. 2011) using the Large Binocular Telescope (LBT) and the Gran Telescopio Canarias (GTC) and in this paper, we present results from our study of the stellar population and variable stars in Andromeda XIX (And XIX; McConnachie et al. 2008), the most extended of Andromeda's dSph companions.

And XIX (R.A.= $00^h19^m32\fs1$, decl. = $+35°02'37\farcs1$, J2000.0; $l = 115\fdg6$, $b = -27\fdg4$; McConnachie et al. 2008) was discovered by McConnachie et al. (2008) in a photometric survey of the southwestern quadrant of M31 performed with the Megaprime camera of the Canada–France–Hawaii Telescope (CFHT). The galaxy is located at a projected distance of ∼120 kpc (Conn et al. 2012) from the center of M31. The discovery data show a steep red giant branch (RGB) but do not reach deep enough to sample the galaxy HB. McConnachie et al. (2008) estimate for And XIX a heliocentric distance of 933 kpc using the luminosity of the RGB tip, however, a closer distance of 821 kpc is derived by Conn et al. (2012) applying a Bayesian approach to the same data to estimate the luminosity of the RGB tip. With a half-light radius of $r_h = 6.2'$ (corresponding to a linear extension of either ∼1.7 or 1.5 kpc depending on whether the McConnachie et al. 2008 or Conn et al. 2012 distance estimate is adopted), And XIX is the largest of Andromeda's dSph companions, as well as the most extended of the Local Group (LG) satellites. In the stellar density map presented by McConnachie et al. (2009), an overdensity of stars named the Southwest Cloud seems to connect And XIX with the halo of M31, providing hints of a possible interaction between And XIX and Andromeda itself. Collins et al. (2013) spectroscopically investigated 27 stars located around the RGB of And XIX measuring a small velocity dispersion when compared to the galaxy radial extent. The authors attributed this "cold" velocity dispersion to the tidal interaction with M31. From the spectra they also derived an average value of the metallicity $[Fe/H] = -1.8 \pm 0.3$ dex using the equivalent width of the calcium triplet and the Starkenburg et al. (2010) method, which is consistent with the value of $[Fe/H] = -1.9 \pm 0.1$ dex found photometrically by McConnachie et al. (2008) by an isochrone-fitting of the galaxy CMD.

Table 1
Log of And XIX Observations

Dates	Filter	N	Exposure Time (s)	Seeing (FWHM) (arcsec)
2010 Oct 8	*B*	2	420	1.5
2010 Dec 1–3	*B*	42	420	0.7
2010 Oct 8–11	*V*	6	420	1.3–2.0
2010 Dec 1	*V*	25	420	0.8

The paper is organized as follows. Observations, data reduction, and calibration of And XIX photometry are presented in Section 2. Results on the identification and characterization of the variable stars, the catalog of light curves, and the Oosterhoff classification of the RR Lyrae stars are discussed in Sections 3 and 4. The distance to And XIX derived from the RR Lyrae stars is presented in Section 5. The galaxy CMD is presented in Section 6. Properties and classification of the variable stars above the HB are discussed in Section 7. In Section 8, an estimate of the contamination from the halo of M31 is given. The discussion on the spatial distribution of And XIX's stars is presented in Section 9. In Section 10, we give an interpretation of the CMD using stellar isochrones and evolutionary tracks. Finally, a summary of the main results is presented in Section 11.

2. OBSERVATIONS AND DATA REDUCTIONS

Time series *B*, *V* photometry of And XIX was obtained in fall 2010 using the Large Binocular Cameras (LBC[6]) mounted at the foci of the LBT. Each LBC consists of an array of four CCDs with total field of view (FoV) of $\sim 23' \times 23'$ and pixel scale of $0\farcs225$ pixel^{-1}. The two LBCs were optimized for the blue and red portion of the visible spectrum. The *B* exposures were obtained with the Blue LBC, whereas the *V* exposures were obtained with the Red LBC. We obtained 44 *B* and 31 *V* images each corresponding to a 420s exposure, for total exposure times of 18480s and 13020s in *B* and *V*, respectively. The log of And XIX observations is provided in Table 1.

[6] See http://lbc.oa-roma.inaf.it/.

Each image was pre-reduced (bias-subtracted, flat-fielded, and astrometrized) by the LBT team through the LBC dedicated pipeline. Point spread function photometry was then performed using the DAOPHOT-ALLSTAR-ALLFRAME package (Stetson 1987, 1994). The alignment of the images was performed using DAOMATCH, one of the routines in the DAOPHOT package, whereas DAOMASTER (Stetson 1992) was used to match point sources. The absolute photometric calibration to Johnson B and V was performed using stars in the scientific fields for which calibrated photometry was available from previous studies. As a first step, we cross-matched our photometric catalogs composed by sources in the four CCDs with the SDSS catalog (Abazajian et al. 2009). The SDSS catalog was queried only for objects flagged as stars by the reduction package, and with good quality of the observations. A total of 1121 stars were found to be common between the two catalogs. The calibration equations available at http://www.sdss.org/dr4/algorithms/sdssUBVRITransform.html were used to convert the g and r magnitudes of the SDSS stars to the Johnson B and V magnitudes. The parameters of the photometric calibration were derived by fitting the data to the equations $B - b = c_B + m_B \times (b - v)$ and $V - v = c_V + m_V \times (b - v)$, where B and V are the standard Johnson magnitudes of the SDSS stars, and b and v are the instrumental magnitudes in our LBC catalog. The fit was performed using a 3σ clipping rejection algorithm. A total of 512 stars were used in the final fit, with magnitudes ranging from 15.7 to 24.3 mag in B, and from 0.2 to 1.7 mag in the $B - V$ color.[7] The final rms of the fit was of 0.04 mag both in B and V.

3. IDENTIFICATION OF THE VARIABLE STARS

The first step in the identification of variable stars was to search for objects with higher values of the variability index computed in DAOMASTER (Stetson 1994). We then also checked for variability all the stars with colors and magnitudes falling within the edges of the RR Lyrae and AC instability strips (ISs), according to the definition by Marconi et al. (2004). The final list of candidate variable stars consisted of ∼300 sources that were all inspected visually using the Graphical Analyzer of Time Series package (GRaTIS), custom software developed at the Bologna Observatory by P. Montegriffo (see, e.g., Clementini et al. 2000). GRaTiS uses both the Lomb periodogram (Lomb 1976; Scargle 1982) and the best fit of the data with a truncated Fourier series (Barning 1963). The majority of the candidate variables were identified in both photometric bands, however, in few cases we only had a reliable light curve in the B band. The period search was performed first on the B band for which we had a larger number of epochs (44 phase-points). Final periods were then derived through an iterative procedure between the two photometric bands. The depth and sampling of the B data is such that we were able to detect variables as faint as $B \sim 26$ mag, with periods ranging from a few hours to several days. A total of 39 bona-fide variable stars were identified, of which 31 were RR Lyrae stars (23 RRab and 8 RRc) lying on the galaxy HB and 8 were classified as ACs, based on luminosities about 1–1.5 mag brighter than the HB level and the comparison with the AC IS, theoretical isochrones, and the Period–Wesenheit (PW) relation (see Sections 7 and 10.2). Among the variables were 5 RR Lyrae stars and 1 AC for which we have reliable data only in the B band. Identification and properties of the confirmed variable stars are summarized in Table 2. Column 1 gives the star identifier. We assigned to the variables an increasing number starting from the galaxy center, for which we adopted McConnachie et al. (2008)'s coordinates. Columns 2 and 3 provide the right ascension and declination (J2000 epoch), respectively. These coordinates were obtained from our astrometrized catalogs. Column 4 gives the type of variability. Columns 5 and 6 list the pulsation period and the Heliocentric Julian Day (HJD) of maximum light, respectively. Columns 7 and 8 give the intensity-averaged mean B and V magnitudes, while Columns 9 and 10 list the corresponding amplitudes of the light variation. Light curves for the 39 stars are shown in Figure 1. To calibrate the photometry of stars that only have B light-curves, we simply added to the instrumental photometry the zero point c_B of the B calibration equation.

The time-series photometry of the variable stars is provided in Table 3, which is published in its entirety in the online journal.

Figure 2 shows the position of the variable stars in the FoV covered by our LBC observations. In the figure black dots mark non-variable stars, red circles and blue triangles mark RRab and RRc stars, respectively, and the ACs are shown by green squares. A black ellipse drawn by convolving the And XIX half-light radius with the galaxy ellipticity and position-angle, as published by McConnachie et al. (2008), delimitates the region containing the bulk of And XIX's stars. In the following we refer to this area as the region within And XIX half-light radius.

4. PERIOD–AMPLITUDE DIAGRAM AND OOSTERHOFF CLASSIFICATION

The right panel of Figure 3 shows the B-band period-amplitude diagram (also known as the Bailey diagram, Bailey 1902) of the RR Lyrae stars identified in this study. Open symbols mark variable stars falling inside the ellipse shown in Figure 2. Variables inside and outside the galaxy half-light radius do not show differences in this plot. Also shown in the figure are the loci defined, respectively, by the bona-fide regular (solid curves) and the well-evolved (dashed curves) fundamental-mode RR Lyrae stars in the Galactic GC M3, from Cacciari et al. (2005). M3 has Oo I properties and its regular RRab stars define the locus occupied by the MW Oo I GCs very well, whereas the evolved RRab stars mimic the locus defined by the MW Oo II GCs. All the RR Lyrae stars identified in this study, independently of being located inside or outside And XIX's half-light radius, fall on either the Oo I locus or between the two lines defined by the M3 variables (Cacciari et al. 2005). The left panel of Figure 3 shows the comparison of And XIX variables with the period-amplitude diagram of the RR Lyrae stars detected in four other M31 dwarf satellites (namely, And I, And II, And III, and And VI). Data for the RR Lyrae stars in And I and And III are from Pritzl et al. (2005), for And II from Pritzl et al. (2004), and for And VI from Pritzl et al. (2002). The variables appear to concentrate mainly toward the Oo I locus or in the region between Oo I and Oo-Int lines, thus suggesting that there is paucity of Oo II satellites around M31.

The average period of the RRab stars inside the ellipse in Figure 2 is $\langle P_{ab} \rangle = 0.610$ days (average on seven stars, $\sigma = 0.03$ days) and becomes $\langle P_{ab} \rangle = 0.62$ days (average on 23 stars, $\sigma = 0.03$ days) if we average over all the RRab stars identified in the present study. This along with the position on the period–amplitude diagram suggests that all the RR Lyrae stars we have identified likely belong to And XIX. The ratio of the number of RRc over total number of RR Lyrae stars is $f_c = 0.26$. Based on these observations, we conclude that And XIX has Oo-Int properties.

[7] The coefficients of the calibration equations are $c_B = 27.532$, $m_B = -0.137$, $c_V = 27.530$, $m_V = -0.0633$.

Table 2
Identification and Properties of the Variable Stars Identified in And XIX

Name	α (2000)	δ (2000)	Type	P (days)	Epoch (Max) JD (2400000)	$\langle B \rangle$ (mag)	$\langle V \rangle$ (mag)	A_B (mag)	A_V (mag)
V1	00:19:36.1	+35:02:25.6	RRab	0.558	55533.592	25.81	25.32	1.49	1.17
V2	00:19:36.0	+35:04:17.5	RRab	0.5856	55477.717	25.86	25.46	0.66	0.53
V3	00:19:32.4	+35:00:35.3	AC	1.306	55477.700	24.29	23.82	1.33	1.06
V4[a]	00:19:38.9	+35:04:47.2	RRab	0.649	55532.600	25.89	...	0.68	...
V5	00:19:34.7	+35:05:30.4	AC	1.043	55476.140	24.46	23.94	0.66	0.61
V6	00:19:21.6	+35:01:01.9	RRc	0.3887	55532.730	25.79	25.31	0.53	0.42
V7[a]	00:19:44.8	+35:02:40.5	RRc	0.3905	55532.682	25.96	...	0.35	...
V8	00:19:18.3	+35:02:05.7	AC	0.5873	55533.583	24.43	23.99	0.87	0.69
V9	00:19:26.3	+34:59:21.7	RRab	0.6159	55533.702	25.77	25.24	0.75	0.60
V10	00:19:41.8	+35:05:20.8	RRab	0.6054	55531.635	25.77	25.27	1.10	0.87
V11	00:19:19.1	+34:59:38.8	RRab	0.6194	55533.592	25.83	25.32	1.16	0.92
V12[a]	00:19:44.1	+35:05:53.5	RRab	0.689	55532.700	25.62	...	0.67	...
V13	00:19:37.9	+35:07:22.3	RRab	0.5860	55477.735	25.86	25.42	0.98	0.78
V14	00:19:23.1	+34:57:08.5	RRc	0.4010	55531.653	25.69	25.26	0.56	0.45
V15	00:19:23.8	+34:56:47.7	RRab	0.5851	55532.790	25.80	25.27	0.77	0.61
V16	00:19:58.1	+35:02:59.6	RRc	0.3748	55531.795	25.74	25.35	0.64	0.51
V17	00:19:58.4	+35:02:57.6	RRab	0.6105	55533.695	25.83	25.42	1.06	0.84
V18	00:19:04.7	+35:02:58.3	RRab	0.6167	55477.723	25.80	25.35	1.17	0.93
V19	00:19:55.0	+34:58:25.6	AC	1.2150	55533.830	24.26	23.87	1.54	1.22
V20	00:19:03.6	+35:00:32.5	AC	1.146	55480.720	24.43	23.86	0.80	0.63
V21	00:19:29.6	+34:55:12.2	RRab	0.6052	55531.686	25.63	25.27	0.89	0.71
V22	00:19:55.5	+35:07:30.1	RRc	0.4090	55531.710	25.76	25.33	0.49	0.45
V23	00:19:29.8	+34:54:39.8	RRc	0.4076	55477.718	25.69	25.26	0.57	0.38
V24	00:19:30.5	+34:54:29.2	AC	0.5839	55533.785	24.90	24.51	1.28	1.02
V25	00:20:06.6	+35:03:54.8	RRab	0.643	55477.717	25.73	25.36	1.02	0.81
V26[a]	00:19:33.3	+35:11:27.7	RRab	0.575	55532.767	25.75	...	1.02	...
V27	00:19:55.8	+34:56:05.9	RRab	0.6653	55532.735	25.57	25.17	1.06	0.85
V28	00:19:47.1	+35:10:59.9	RRab	0.6423	55531.742	25.88	25.34	1.07	0.85
V29[a]	00:20:10.9	+35:04:53.5	RRab	0.6164	55531.780	25.74	...	0.81	...
V30	00:18:51.7	+35:04:34.1	RRab	0.6291	55477.106	25.73	25.25	1.21	0.96
V31	00:20:10.4	+35:07:30.4	RRab	0.6433	55533.793	25.82	25.42	0.85	0.69
V32	00:18:58.6	+34:55:38.4	AC	1.0513	55477.790	24.47	24.10	1.15	0.92
V33	00:18:59.7	+35:10:21.1	RRab	0.640	55533.733	26.15	25.65	1.11	0.88
V34	00:20:16.9	+35:02:24.0	RRab	0.6439	55531.670	25.83	25.35	0.66	0.52
V35	00:19:26.9	+35:14:24.9	RRc	0.330	55532.790	25.84	25.44	0.77	0.62
V36[a]	00:20:03.2	+35:12:33.9	AC	0.6230	55532.650	24.55	...	0.48	...
V37	00:18:40.8	+35:05:14.3	RRab	0.6070	55531.669	25.82	25.30	1.50	1.19
V38	00:18:59.3	+35:12:59.7	RRc	0.4310	55533.810	25.59	25.21	0.33	0.32
V39	00:20:19.7	+34:52:48.8	RRab	0.5787	55532.750	25.64	25.31	0.75	0.60

Note. [a] Only B light curves are available for these stars. The $\langle B \rangle$ values were obtained by adding to the instrumental $\langle b \rangle$ values the zero point of the B calibration equation.

5. DISTANCE

We measured the distance to And XIX using its RR Lyrae stars. The average V magnitude of the RR Lyrae stars is $\langle V(\mathrm{RR}) \rangle = 25.34$ mag ($\sigma = 0.10$ mag, average over 26 stars). If we consider only RR Lyrae stars inside the galaxy half-light radius (ellipse in Figure 2; namely, the seven RRab stars: V1, V2, V4, V9, V10, V11, V12; and the two RRc stars V6, V7) the average becomes $\langle V(\mathrm{RR}) \rangle = 25.32$ mag ($\sigma = 0.07$ mag, average over nine stars). The difference between the two average values is negligible, thus further confirming that all the RR Lyrae stars we have identified likely belong to And XIX. In the following, we will use the average over all the RR Lyrae stars as more representative of the whole galaxy. The $\langle V(\mathrm{RR}) \rangle$ value was de-reddened using a standard extinction law ($A_V = 3.1 \times E(B-V)$) and as a first approach the reddening value $E(B-V) = 0.066 \pm 0.026$ mag provided by Schlegel et al. (1998) maps. We then assumed an absolute magnitude of $M_V = 0.54 \pm 0.09$ mag for RR Lyrae stars at [Fe/H] $= -1.5$ dex (Clementini et al. 2003; this is consistent with a distance modulus for the Large Magellanic Cloud, LMC, of 18.52 ± 0.09 mag) and corrected for the different metal abundance using the relation $\Delta M_V/\Delta[\mathrm{Fe/H}] = 0.214 \pm 0.047$ mag dex^{-1} by Clementini et al. (2003) and Gratton et al. (2004). We adopted for And XIX the metallicity [Fe/H] $= -1.8 \pm 0.3$ dex derived spectroscopically by Collins et al. (2013). The distance modulus of And XIX derived under the above assumptions is $(m-M)_0 = 24.66 \pm 0.17$ mag. An independent reddening estimate can be obtained from the RR Lyrae stars using Piersimoni et al.'s (2002) method, which is based on the relation between intrinsic $(B-V)_0$ color, period, metallicity, and the B amplitude of the RRab stars. Using the 19 RRab stars for which we have photometry in both the B and V bands, we obtain $E(B-V) = 0.11 \pm 0.06$ mag. The distance modulus derived with this new reddening is $(m-M)_0 = 24.52 \pm 0.23$ mag. Both our distance moduli place And XIX almost at the same distance of M31 and both are in good agreement, within the errors, with the value of $(m-M)_0 = 24.57^{+0.08}_{-0.43}$ mag found by

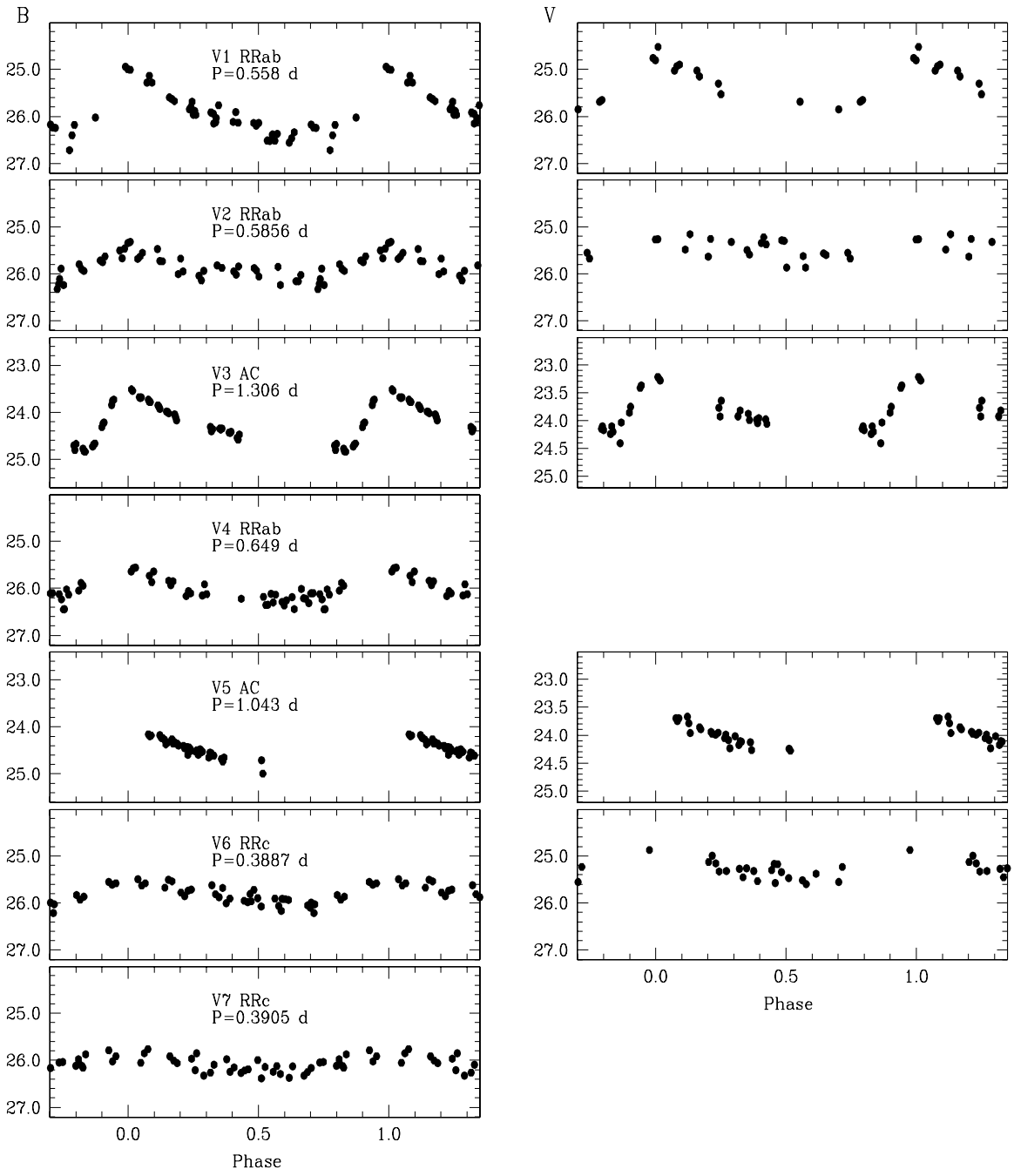

Figure 1. *B* (left panels) and *V* (right panels) light curves of the variable stars identified in And XIX. Stars are ordered with increasing distance from the galaxy center, for which we adopted the McConnachie et al. (2008) coordinates. Typical internal errors for the single-epoch data are in the range of 0.04–0.12 mag in *B*, and of 0.08–0.19 mag in *V*.

Conn et al. (2012). Our estimates are smaller than McConnachie et al. (2008) modulus for And XIX, but still consistent with their value within 1σ.

6. THE CMD

Figure 4 shows the CMDs obtained in the present study selecting objects in different regions of the Field of View (FoV).

To avoid contamination from background galaxies and peculiar objects, we selected our photometric catalog using the χ and Sharpness parameters provided by ALLFRAME. We only retained sources for which $-0.3 \leqslant$ Sharpness $\leqslant 0.3$, and with $\chi < 1.0$ for magnitudes fainter than $V = 22.0$ mag, and $\chi < 1.5$ for magnitudes brighter than $V = 22.0$ mag. These selections led to a total of ∼9000 stars, plotted as dots in Figure 4. The variable stars are plotted in Figure 4 according to their intensity-average magnitudes and colors; red circles were used for the RRab stars, blue triangles for the RRc stars, and green squares for the ACs. Only 26 RR Lyrae stars and 7 ACs could be plotted, as we lack *V* photometry for 5 RR Lyrae stars and 1 AC. The right panel of Figure 4 shows the CMD of the whole FoV of the LBC observations; the 1σ error bars, as derived from artificial star tests conducted on real images, are also drawn. The left panel shows only the stars inside the ellipse drawn with the galaxy half-light radius ($r_h = 6\farcm2$; McConnachie et al. 2008; see Figure 2), and the central panel shows the CMD of the stars inside the elliptical ring with internal radius $6\farcm2$ and external radius $8\farcm8$, which encloses the same area as in

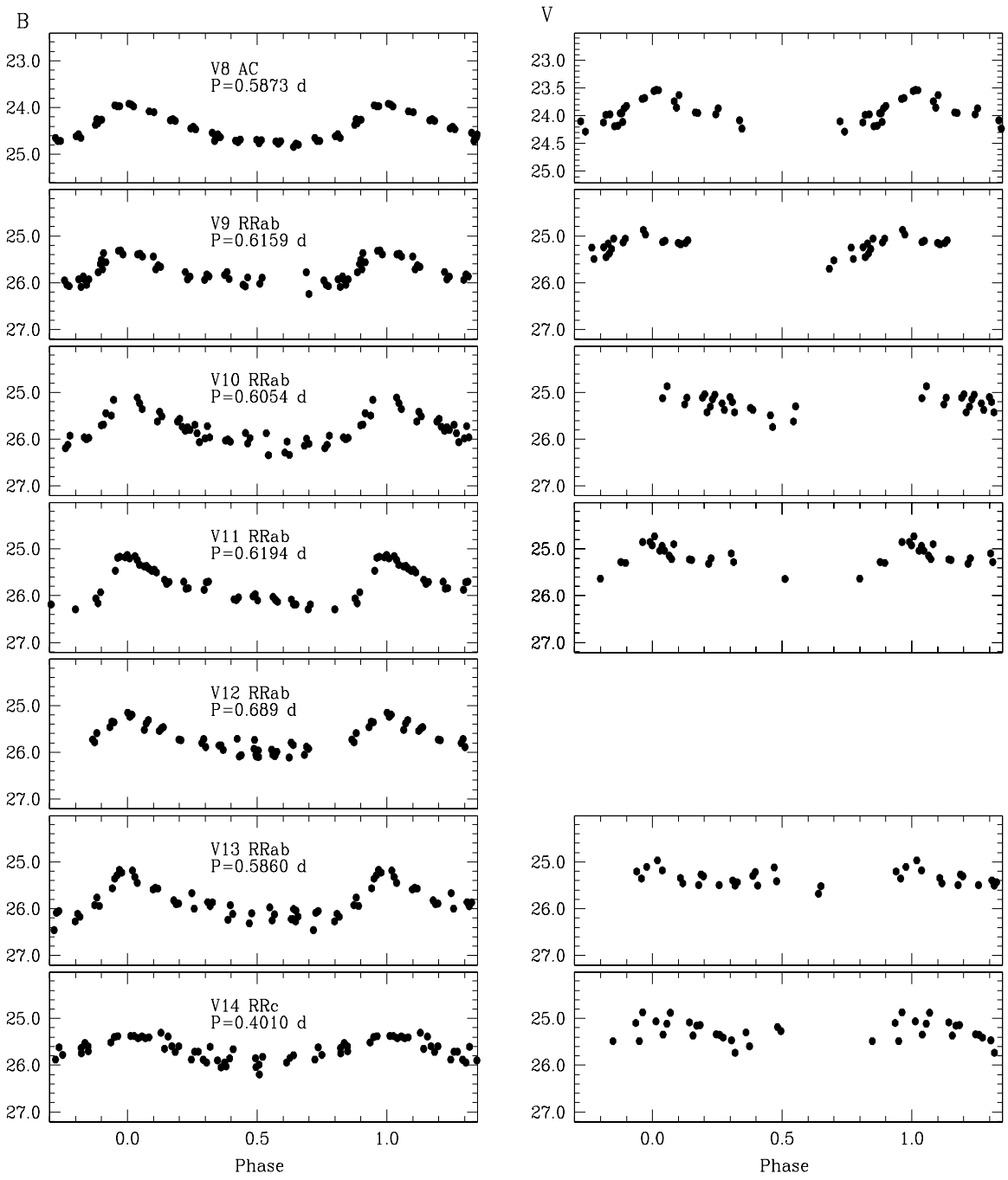

Figure 1. (Continued)

the left panel. The most prominent features of the And XIX CMD are

1. a RGB, between $B-V=0.6$–1.5 mag, extending upward to $V\approx 22$–22.5 mag;
2. a red HB with colors $0.6<B-V<0.8$ mag;
3. a distribution of sources extending nearly vertically at $B-V\sim 0.2$–0.4 mag; the unusual color of these objects (see Section 9), can be explained by unresolved background galaxies; and
4. a sequence of stars at $B-V\sim 1.5$–1.7 mag and extending blueward around $V=22$ mag. This feature is likely composed by foreground field stars (also see Section 9).

In the left and center panels of Figure 4, we have plotted in blue the ridge lines of the Galactic globular cluster NGC 5824 from Piotto et al. (2002), corrected to the distance and reddening of And XIX that we derived from the RR Lyrae stars (see Section 5). We assumed for NGC 5824 a distance modulus of $(m-M)_0=17.54$ mag and a reddening of $E(B-V)=0.13$ mag from the Harris (1996) catalog (2010 edition). NGC 5824 has a metallicity [Fe/H] $=-1.94\pm0.14$ dex (Carretta et al. 2009) that is very similar to the metal abundance of And XIX estimated by Collins et al. (2013). The RGB of NGC 5824 matches And XIX's RGB very well thus confirming both the similar metallicity and the higher reddening value inferred from the RR Lyrae stars. The IS boundaries for RR Lyrae stars and ACs with $Z=0.0002$ from Marconi et al. (2004) are overplotted to the CMD in the right panel of Figure 4. The variables we have classified as RR Lyrae stars fall well inside the boundaries of the RR Lyrae IS, confirming they are bona-fide RR Lyrae stars. Similarly, the

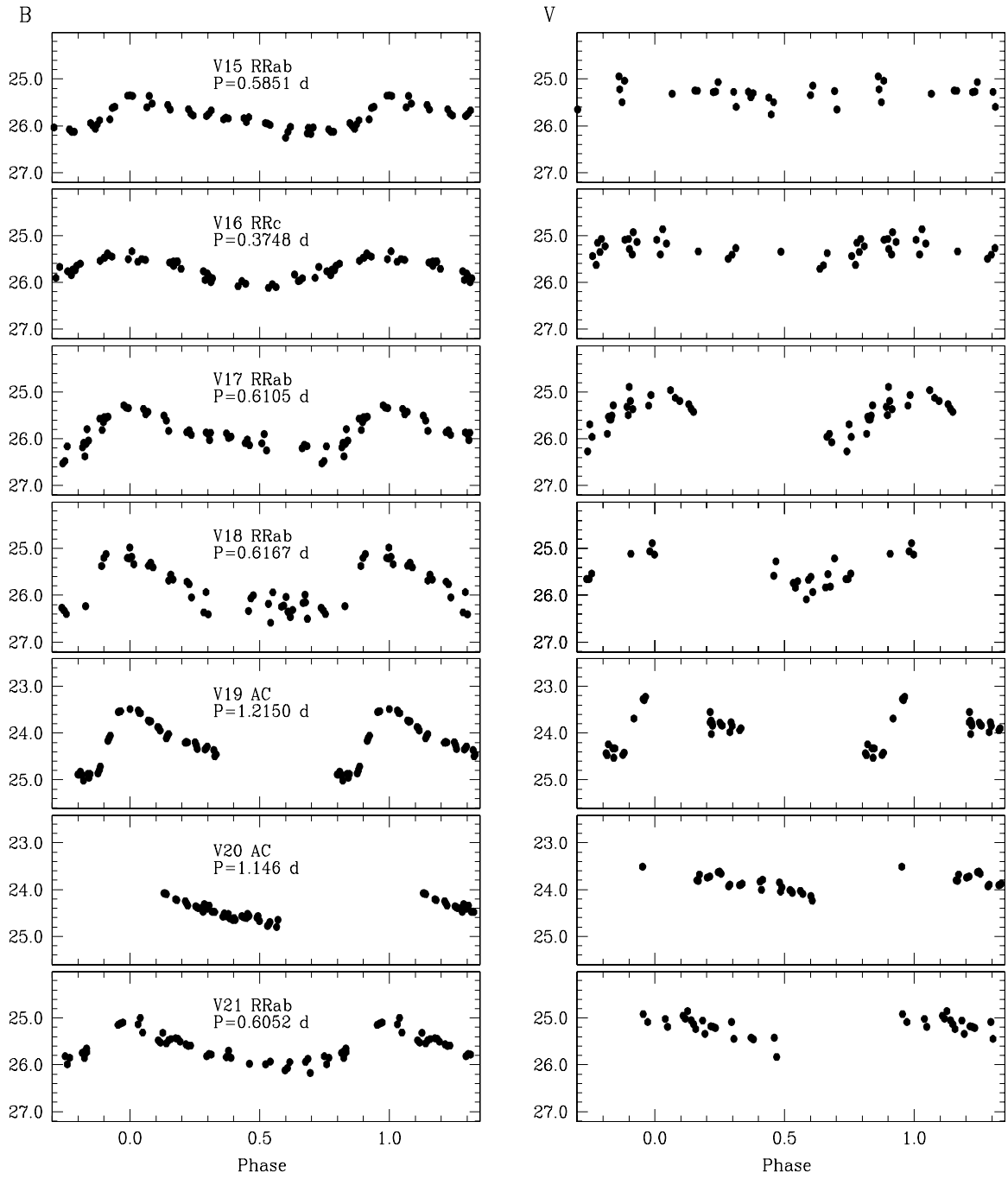

Figure 1. (Continued)

variables above the HB appear to be confined in the region of the CMD where ACs are usually found (see the following section).

7. ANOMALOUS CEPHEIDS

In And XIX, we have identified eight variable stars from about 1 to 1.5 mag brighter than the average B magnitude of the HB. These stars are found to fall inside the boundaries of the IS for ACs from Marconi et al. (2004; see Figure 4), thus providing support to their classification as ACs. In order to investigate their nature further, we have also compared them with the period–luminosity (PL) relations for ACs. ACs follow a PL relation that differs from both the Classical Cepheids and the type II Cepheids PL relationships (see Figure 1 of Soszynski et al. 2008a). Unfortunately, the PL relation has the disadvantage of being reddening dependent and in some cases the scatter around the mean value can be very high. Narrower relations are found introducing a color term in the PL relation and in particular the Wesenheit function (van den Bergh 1975; Madore 1982) includes a color term whose coefficient is equal to the ratio between total-to-selective extinction in a filter pair. In such a way, the PW relation is reddening free by definition. The Wesenheit index in our case is $W(B, V) = M_V - 3.1 \times (B - V)$, where M_V is the V magnitude corrected for the distance. We have B and V magnitudes for seven of the variables above the HB. Their $\langle V \rangle$ magnitudes were corrected using the distance modulus $(m - M)_0 = 24.52$ mag derived from the RR Lyrae stars and used to derive the corresponding Wesenheit indices. The position of these seven variables in the PW plane is shown

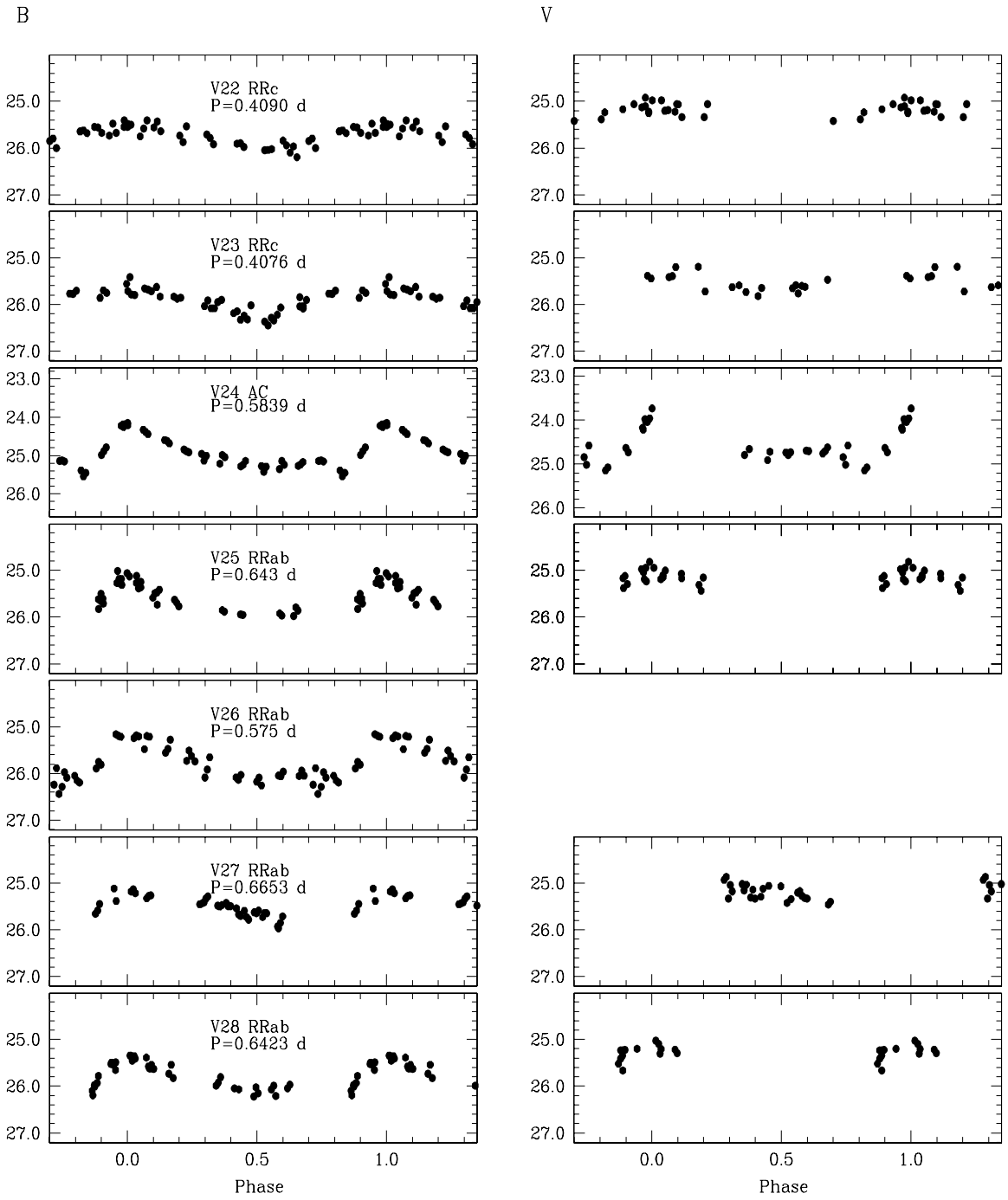

Figure 1. (Continued)

in the left panel of Figure 5, where we also plot, as solid lines, the PW relations for ACs recently derived by Ripepi et al. (2013) using 25 ACs in the LMC[8]. Six of the And XIX bright variables appear to fall well on the Ripepi et al.'s (2013) PW relations for ACs with stars V3, V19, and V32 likely being fundamental-mode pulsators, and stars V5, V20, and V24 likely pulsating in the first-overtone mode. On the other hand, star V8 appears to be more than 2σ off the first-overtone PW relation, hence its classification as AC seems to be less robust. To demonstrate that these bright variables are mostly ACs, the PW relation for Classical Cepheids (CCs) in the LMC derived by Soszynski et al. (2008b) is shown on the right panel of Figure 5. The PW relation for CCs indeed does not fit the bright variables in And XIX very well.

We will further discuss the nature of the bright variables of And XIX in Section 10.2 where we compare them with theoretical isochrones.

Mateo et al. (1995) found that the specific frequency of ACs (i.e., the number of ACs per 10^5 L_V) in the Galactic dSph galaxies is related to the luminosity and metallicity of the parent dSph. Pritzl et al. (2004, 2005) found that this correlation also holds for M31's satellites And I, And II, And III, and And VI. On the assumption that the eight supra-HB variables of And XIX are ACs, in Figure 6, we plot the specific frequency of ACs in And XIX versus its luminosity (left panel) and metallicity (right

[8] Ripepi et al.'s (2013) relations were derived for the V and I bands, and we have converted them to B and V using Equation (12) of Marconi et al. (2004).

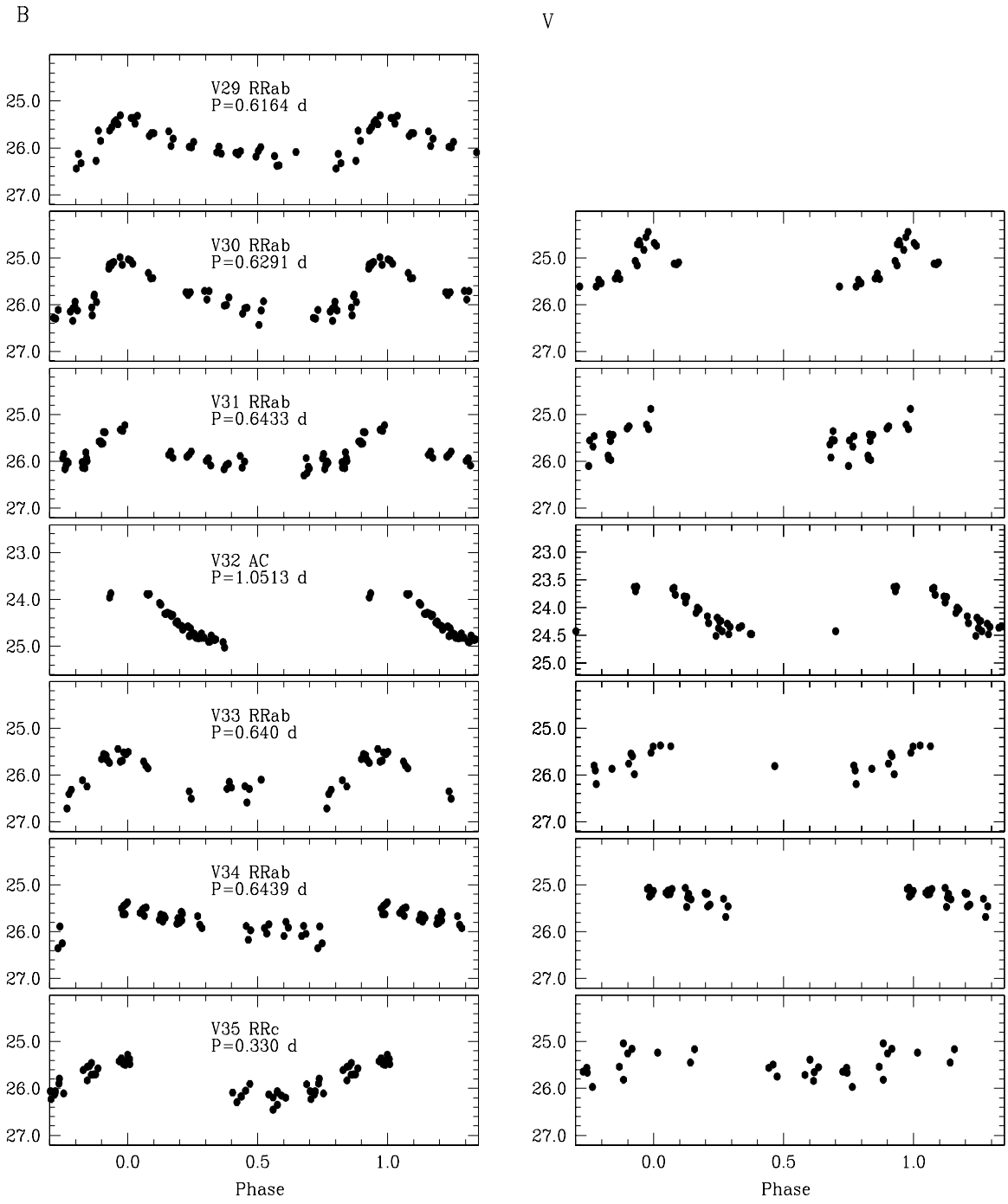

Figure 1. (Continued)

panel) and compare it to the one in Galactic and M31 dSphs from Pritzl et al. (2004). And XIX follows well the relation traced by the other dSphs. This also indicates that we have detected almost all the short period variable stars at $V \sim 24$ mag in And XIX, as also dictated by the artificial star test that gives a completeness of ∼80% at this level of magnitude.

8. M31 HALO CONTAMINATION

Although And XIX is far (∼120 kpc; Conn et al. 2012) from the M31 center, the contamination from RR Lyrae stars and ACs belonging to the M31 halo may be not negligible. The FoV of the LBC (∼0.15 deg^2) is such that we were able to fit in just one pointing a large portion of And XIX ($\simeq 2 \times r_h$). Unfortunately, in such a large FoV, contaminants are also expected to be present in a large number. As we showed in Section 5, And XIX is almost at the same distance of M31 and for this reason the luminosity of the variable stars in And XIX and in the M31 halo is similar, thus distinguishing the two samples on the basis of the average luminosity is not possible. To estimate how many variable stars belonging to the M31 halo can be expected to contaminate And XIX's sample, we used the results from the search for variable stars in six fields around M31 made by Jeffery et al. (2011) using *HST*/ACS. Two of these fields are in the halo of M31

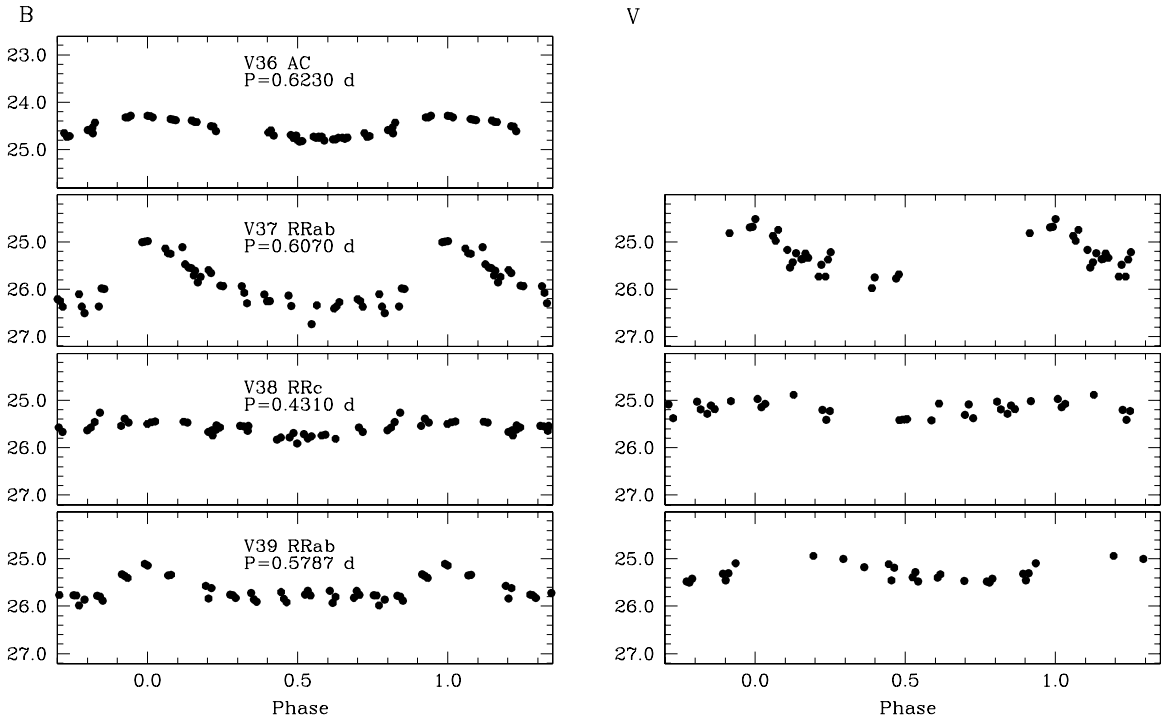

Figure 1. (Continued)

Table 3
B, *V* Photometry of the Variable Stars Detected in And XIX

And XIX–Star V1–RRab					
HJD (−2,455,000)	B (mag)	σ_B (mag)	HJD (−2,455,000)	V (mag)	σ_V (mag)
477.72208	26.03	0.30	531.66930	25.69	0.23
531.65805	26.51	0.30	531.75167	25.85	0.18
531.66338	26.52	0.24	531.79774	25.69	0.19
531.66935	26.39	0.27	531.80311	25.65	0.27
531.70489	26.56	0.32	533.58629	24.76	0.14
531.71021	26.47	0.35	533.59162	24.81	0.13
531.71570	26.34	0.24	533.59698	24.52	0.15
531.75178	26.17	0.18	533.63227	25.02	0.08
531.75713	26.24	0.18	533.63763	24.93	0.10
531.76244	26.25	0.16	533.64302	24.90	0.07

(This table is available in its entirety in a machine-readable form in the online journal. A portion is shown here for guidance regarding its form and content.)

at a distance of about 35 kpc from the center in the southeast direction along the galaxy minor axis. They were found to contain five and no RR Lyrae stars, respectively, despite having comparable stellar density. Furthermore, neither of the two halo fields were found to contain ACs. From these results we can give a rough estimate of how many RR Lyrae stars and ACs belonging to M31 we expect to find in the field of And XIX. Assuming a stellar density of the M31 halo of $\propto r^{-3.2}$ (Gilbert et al. 2012) and after scaling for the different area surveyed by the LBC and *HST*/ACS we estimated a contamination from the M31 halo by five RR Lyrae and no ACs. Even if these could be underestimates, the number of possible contaminants from M31 appears to be small compared to the 31 RR Lyrae stars and eight ACs we have found in And XIX. On the basis of the arguments above, we conclude that the contamination from M31 halo does not significantly affect our results.

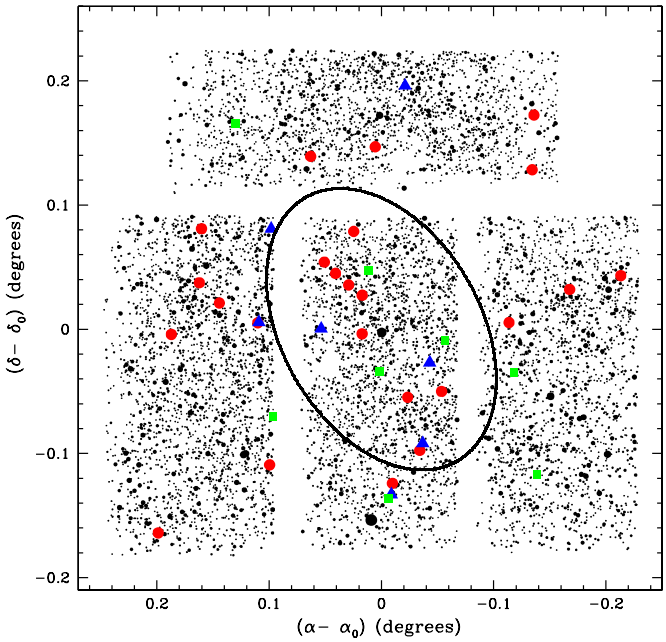

Figure 2. Spatial distribution of the variable stars identified in the FoV covered by our LBC observations of And XIX. The red circles and blue triangles mark RRab and RRc stars, respectively. The green squares are ACs. The black dots are non-variable stars; they are plotted with symbol sizes inversely proportional to their magnitude. The black ellipse is drawn by convolving the And XIX half-light radius with the galaxy ellipticity and position-angle following McConnachie et al. (2008).

(A color version of this figure is available in the online journal.)

9. SPATIAL DISTRIBUTION

In order to explore the spatial structure of And XIX, Figure 7 shows the spatial distributions of stars from different regions of the CMD (Figure 8). To better visualize the maps, the data points were binned to a pixel size of 7 arcsec and smoothed

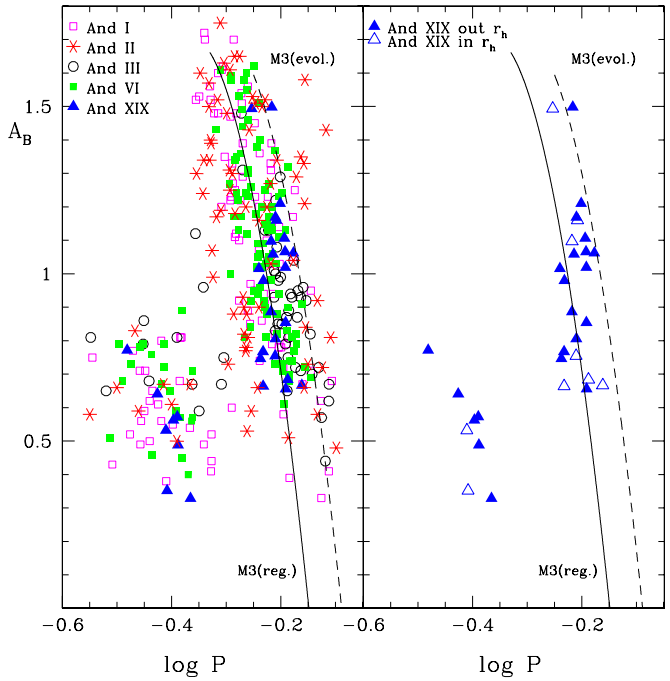

Figure 3. Right: period–amplitude diagram in the *B* band for the RR Lyrae stars identified in the present study. The open symbols mark variables falling inside the ellipse shown in Figure 2. Also shown, for comparison, are the loci defined by the bona-fide regular (solid curve) and well-evolved (dashed curve) fundamental-mode RR Lyrae stars in M3, from Cacciari et al. (2005). Left: comparison of And XIX variables with the RR Lyrae stars identified in four other M31 dwarf satellites (namely, And I, And II, And III, and And VI).

(A color version of this figure is available in the online journal.)

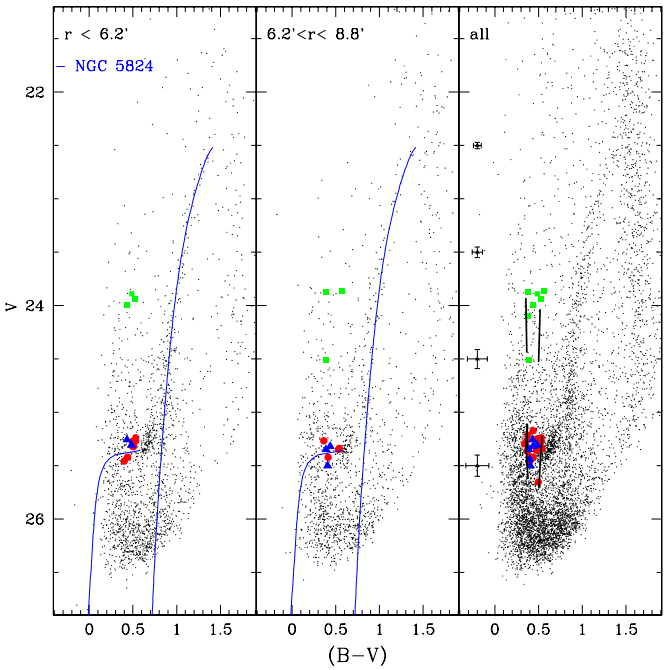

Figure 4. CMDs obtained selecting objects in different regions of the FoV. Only the sources for which $-0.3 \leqslant$ Sharpness $\leqslant 0.3$ and $\chi < 1.0$ for magnitudes fainter than $V = 22.0$ mag, and $\chi < 1.5$ for magnitudes brighter than $V \sim 22.0$ mag, are displayed in the three panels of the figure, in order to reduce contamination from background galaxies and peculiar objects. The red circles are RRab stars, blue triangles are RRc stars, and green squares are ACs. Left: CMD of only stars inside an ellipse drawn with the galaxy half-light radius (see Figure 2). Shown in blue are the ridgelines of the Galactic globular cluster NGC 5824 ([Fe/H] = −1.94 dex; Carretta et al. 2009); middle: same as in the left panel, but for stars inside an elliptical ring with internal radius 6.′2 and external radius 8.′8, which encloses the same area as in the left panel; right: CMD of stars in the whole LBC FoV. The black solid lines show the boundaries of the IS for RR Lyrae stars and ACs with $Z = 0.0002$, from Marconi et al. (2004).

(A color version of this figure is available in the online journal.)

with a two-dimensional Gaussian kernel with $\sigma = 20$ arcsec. In Figure 7, from the top left panel clockwise, we show MW (green symbols in Figure 8) stars, And XIX RGB and HB stars (magenta symbols in Figure 8), intermediate color objects (blue symbols in Figure 8), and blue objects (cyan symbols in Figure 8). Variable stars (red circles for RR Lyrae stars, and green squares for ACs) are also overlaid on the density maps.

As expected, the MW stars are homogeneously distributed all over the field. RGB and HB stars, however, seem to be concentrated along a diagonal bar-like structure running from southwest to northeast and pointing toward the M31 center. Along this bar are also positioned 20 of the 39 variable stars. Interestingly, the distribution of the blue objects does not correlate with the distribution of RGB and HB stars, which are clearly members of And XIX, but instead shows an overdensity in the upper CCD of the LBC camera, in a region around R.A. = 4.°84, decl. = +35.°22, and radius ∼2.5 arcmin. We suggest that these blue objects are most likely unresolved galaxies. To examine this possibility in depth, we calculated an upper limit for the number of unresolved galaxies expected in the FoV of our LBC observations using the *HST* Ultra Deep Field (UDF) catalog of galaxies by Coe et al. (2006) and making the assumption that the distribution of galaxies in the sky is almost isotropic. In the UDF catalog, we selected galaxies with the same range of colors and magnitudes used to select the blue objects in our CMD. Furthermore, we selected galaxies with radii smaller than 0.75 arcsec, which, given the average seeing of the LBC images, should result in unresolved objects. After scaling for the different area surveyed by the UDF catalog of Coe et al. (2006) and by the LBC, we end up with an estimated upper limit of 1450 unresolved galaxies in the LBC field. The number of blue objects in the LBC catalog is 1736, which is comparable to the upper limit found from the UDF catalog. This seems to support our claim that the majority of the blue objects in the CMD are likely unresolved galaxies. As further evidence, Figure 9 shows isochrones with solar metallicities overlaid to the CMD. This figure shows that the blue sources in the CMD (in cyan in Figure 8) are much redder than solar isochrones and are thus more consistent with unresolved galaxies than single stars. In this case, the overdensity in the upper CCD is likely a cluster of galaxies. We searched the Wen & Han (2013) catalog for known clusters of galaxies around the center of the overdensity (∼R.A.= 4.°84, decl. = 35.°22), but did not find any in a radius of ∼2.5 arcmin. However, we noticed that the Wen & Han (2013) catalog is based on SDSS data, which are shallower when compared to our deep photometry.

Finally, the distribution of intermediate color objects partially overlaps with the RGB/HB distribution (which is peaked in the central CCD), but also shows mild overdensities in the upper and right hand CCDs. This sample is likely mostly populated by unresolved galaxies, although there are probably also some members of And XIX. Indeed, the ACs are in this region of the CMD and are contributing to these overdensities. However, only high resolution observations with *HST* will allow a better galaxies/stars separation, thus helping to clarify whether or not And XIX hosts an intermediate/young age component.

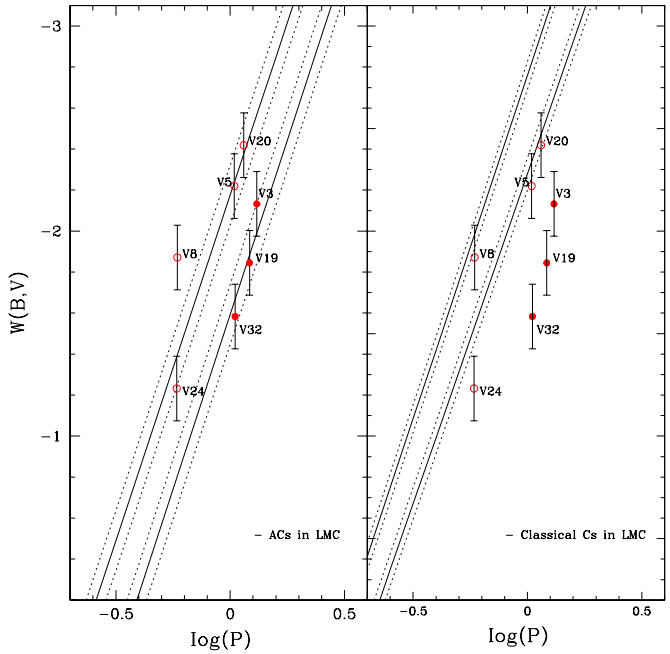

Figure 5. Left panel: PW relations for And XIX's variables brighter than the HB. The solid lines are the fundamental-mode (lower line) and the first-overtone (upper line) PW relations for ACs by Ripepi et al. (2013; converted to B, V bands using the relations in Marconi et al. 2004), with their related 1σ uncertainties. Right panel: same as left panel, but with the PW relations for Classical Cepheids by Soszynski et al. (2008b).

(A color version of this figure is available in the online journal.)

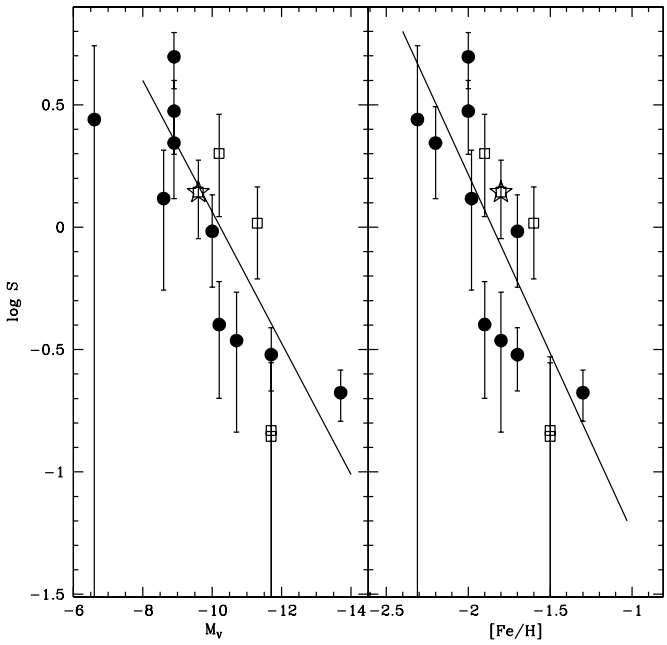

Figure 6. Specific frequency of ACs in MW (filled circles) and M31 (open squares) dSphs versus absolute visual magnitude (M_V, left panel) and metallicity ([Fe/H], right panel) of the parent galaxy. And XIX is marked by a star symbol.

10. CMD INTERPRETATION

10.1. Old Population: Two Episodes of Star Formation

Overlaid on the CMD in Figure 10 are shown the Padova isochrones of different ages and metallicities obtained using the CMD 2.5 web inferface[9] based on models from Bressan et al. (2012). The adopted foreground reddening and the distance modulus are $E(B-V) = 0.11$ mag and $(m-M)_0 = 24.52$ mag, respectively, as derived from the RR Lyrae stars. Although the age–metallicity degeneracy makes the interpretation of the RGB color troublesome, we can still find feasible scenarios by fitting the RGB and HB simultaneously. Our findings suggest that And XIX hosts two distinct stellar populations.

1. An old and metal poor component, hereinafter P1, as suggested by the presence of RR Lyrae stars. Our fit suggests that only metallicity $Z = 0.0003$ ($\log Z/Z_\odot = -1.80$) and ages between 12 and 13 Gyr can fully match the location of the RGB and the average color of the RR Lyrae stars. Formally, we can rule out younger ages (the top right panel illustrates a 11 Gyr isochrone), because the corresponding RGB and HB are too blue and too red respectively, and higher metallicities ($Z = 0.0004$, $\log Z/Z_\odot = -1.67$; middle panels), because the predicted HB is clearly redder than the RR Lyrae color.
2. A more metal rich and possibly younger component, hereafter P2, as traced by the red HB. Based on the isochrone fitting, as shown in middle and bottom panels of Figure 10, we find that isochrones in the metallicity range $Z = 0.0004$–0.0006 ($\log Z/Z_\odot = -1.67/-1.5$), with ages spanning from 6 to 10 Gyr, match well both the color extension of the red HB and the mean position of the RGB. However, the lowest metallicity isochrones actually fit best, while the more metal rich isochrones predict giants that are too red. Lowering the age of the isochrone (<6 Gyr) partially counters this effect, but also produces a too bright HB. Vice versa, isochrones older than 10 Gyr at $Z = 0.0004$, although producing tolerably good fits in the RGB region, miss the red HB.

Unfortunately, the strong galactic contamination makes it difficult to quantify the fraction of blue HB stars. Likewise, the ratio between P1's and P2's star formation (SF) rates is very uncertain.

10.2. A Recent Episode of Star Formation?

The presence of pulsating stars brighter than RR Lyrae stars raises the question of whether And XIX was forming stars up to 1 Gyr ago. In Figures 11 and 12, we show stellar evolutionary tracks from the Basti Web site[10] based on models by Pietrinferni et al. (2004) for metallicities $Z = 0.0003$ and $Z = 0.0006$, respectively, and masses in the range 0.8–2.4 $M_\odot$, overlaid on the observed CMD. We used the Basti tracks for this comparison because the $Z = 0.0003$ and $Z = 0.0006$ metallicities are not available for the Padova evolutionary tracks. In the $Z = 0.0003$ case, the location of the pulsating stars is bracketed by 1.8 and 2.0 $M_\odot$ tracks, while in the $Z = 0.0006$ case it is constrained by 2.0 and 2.2 $M_\odot$ tracks. In terms of age, the best fitting isochrones (see Figure 13) suggest a range of ages 1–1.25 Gyr old at $Z = 0.0003$ and 0.75–1 Gyr old at $Z = 0.0006$. Although this is not a large difference, we note that in the former scenario the pulsating stars are consistent with being ACs, as suggested by the RGB tip of similar luminosity for both the 1.8 and 2.0 $M_\odot$ tracks (both masses are lower than the RGB transition mass), while in the latter they are at the border line between being ACs and short-period Classical Cepheids, as suggested by the short RGB of the 2.2 $M_\odot$ track compared to the 2.0 $M_\odot$ track

[9] http://stev.oapd.inaf.it/cgi-bin/cmd

[10] http://albione.oa-teramo.inaf.it/

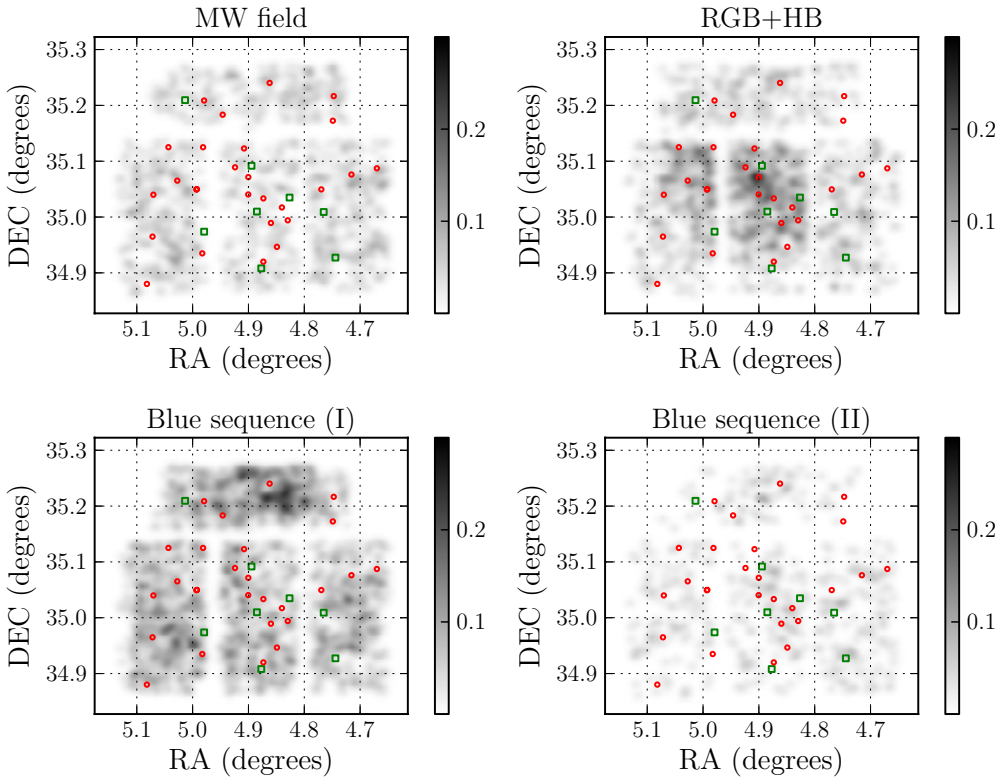

Figure 7. Density-contours of the objects selected using the CMD in Figure 8. From the upper left panel, clockwise, MW stars (in green in Figure 8), RGB+HB stars (in magenta in Figure 8), intermediate blue sequence objects (in blue in Figure 8), and blue sequence objects (in cyan in Figure 8). The red circles are RR Lyrae stars and the green squares are ACs.

(A color version of this figure is available in the online journal.)

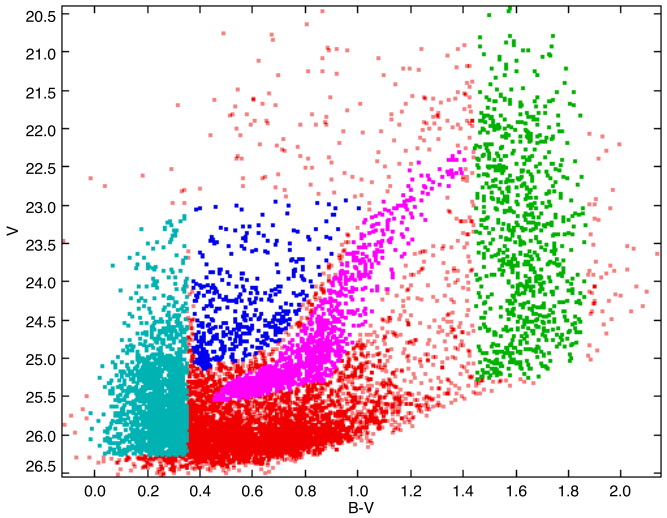

Figure 8. CMD of the sources in the FoV of our observations of And XIX satisfying the χ and Sharpness conditions described in Section 6 (red points), with the selections used to construct the spatial maps of Figure 7 marked in different colors: RGB+HB stars (magenta), MW stars (green), blue objects (cyan), and intermediate blue objects (blue).

(A color version of this figure is available in the online journal.)

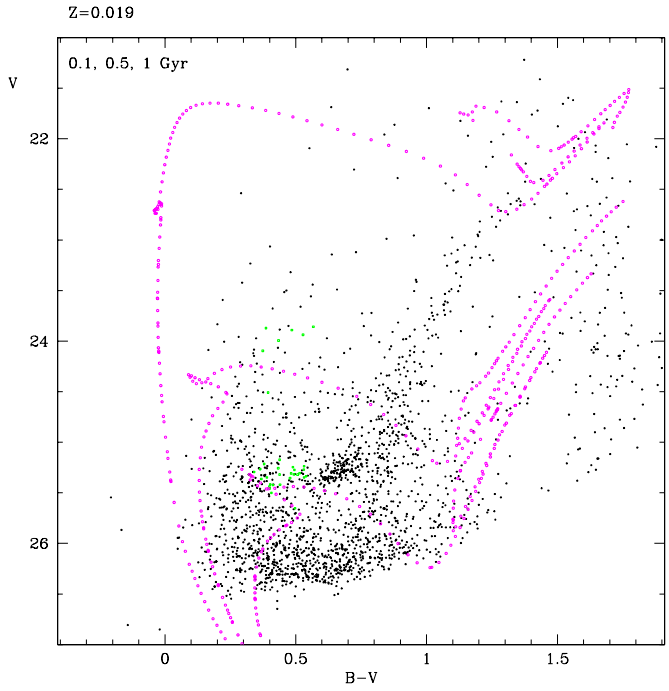

Figure 9. CMD with overlaid solar metallicity isochrones from 0.1 to 1 Gyr.

(A color version of this figure is available in the online journal.)

(the 2.2 $M_{\odot}$ is above the RGB transition mass, the 2.0 $M_{\odot}$ is below). Furthermore, the stellar evolutionary tracks predict the existence of ACs only for metallicities lower than $Z = 0.0004$ (see, e.g., Marconi et al. 2004).

To further investigate the presence of young stars, two synthetic populations (see Cignoni & Tosi 2010, for an overview of the technique) were generated following the two most likely scenarios, namely a metallicity $Z = 0.0006$ and a constant SF in the range 1–0.75 Gyr, and a metallicity $Z = 0.0003$, and a constant SF in the range 1.25–1.00 Gyr. For both models

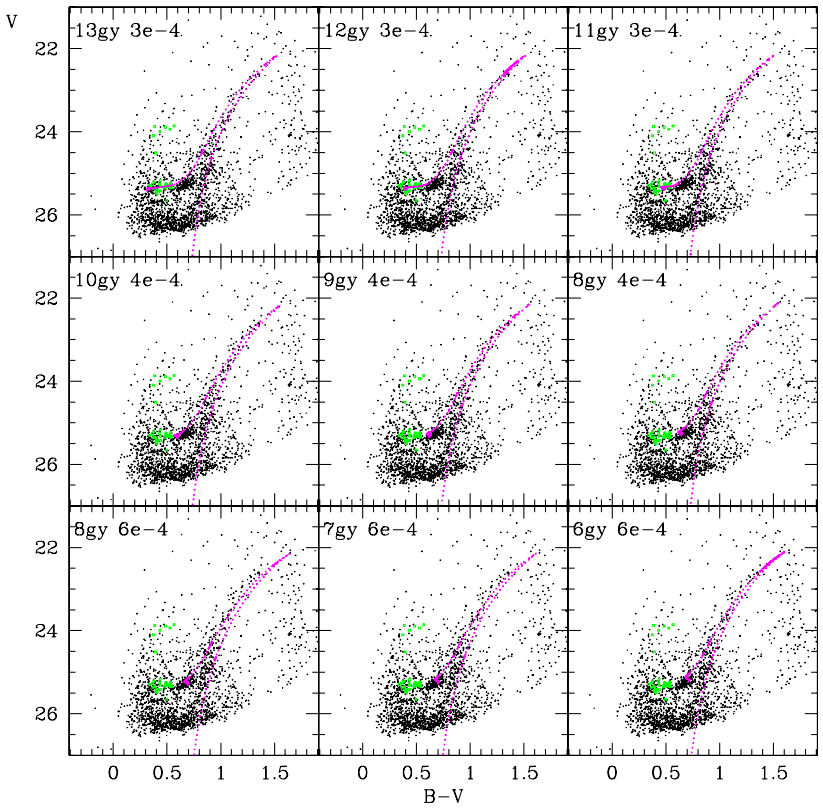

Figure 10. Observed CMD with overlaid stellar isochrones from the Padova evolutionary models on the CMD 2.5 web interface. Metallicities from the top to the bottom panel are $Z = 0.0003$, 0.0004, and 0.0006, respectively. The ages of the isochrones are indicated in each individual panel. Variable stars are represented by the green squares.

(A color version of this figure is available in the online journal.)

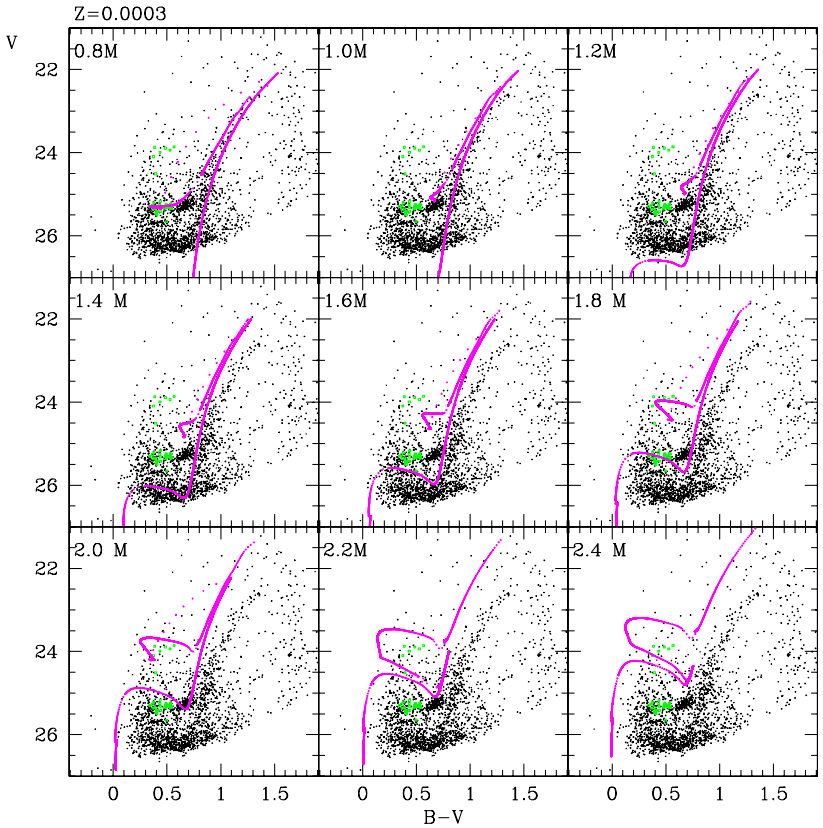

Figure 11. Stellar evolutionary tracks from the Basti Web site. Starting from the top-left to the bottom-right masses from 0.8 to 2.4 $M_{\odot}$. The metallicity is $Z = 0.0003$. Variable stars are represented with green squares.

(A color version of this figure is available in the online journal.)

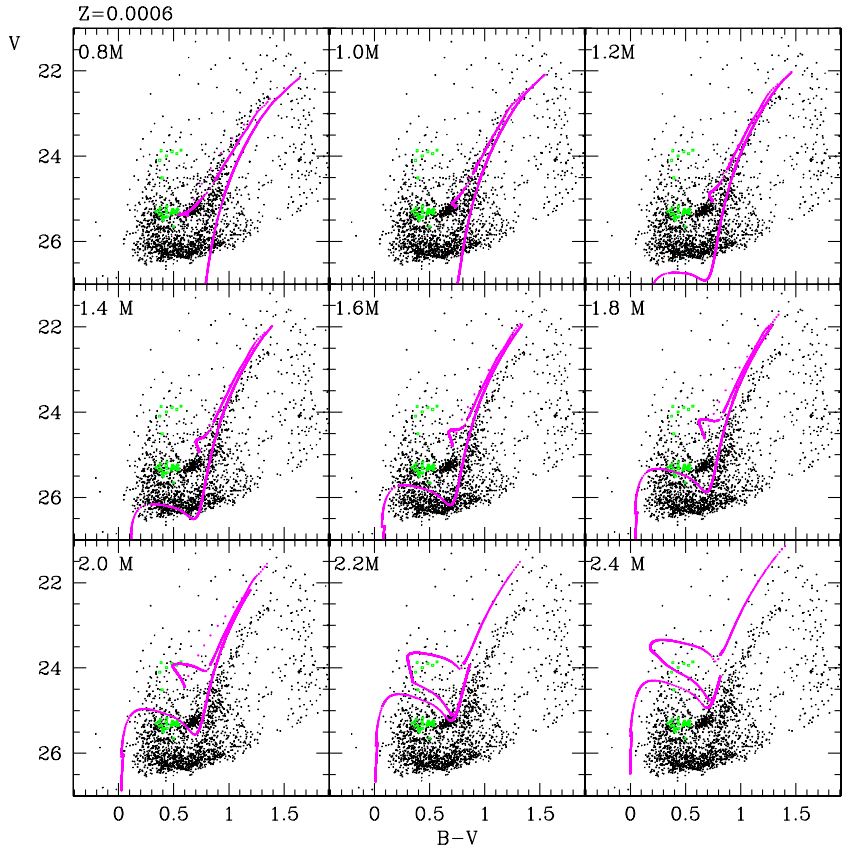

Figure 12. Same as Figure 11, but for metallicity $Z = 0.0006$.
(A color version of this figure is available in the online journal.)

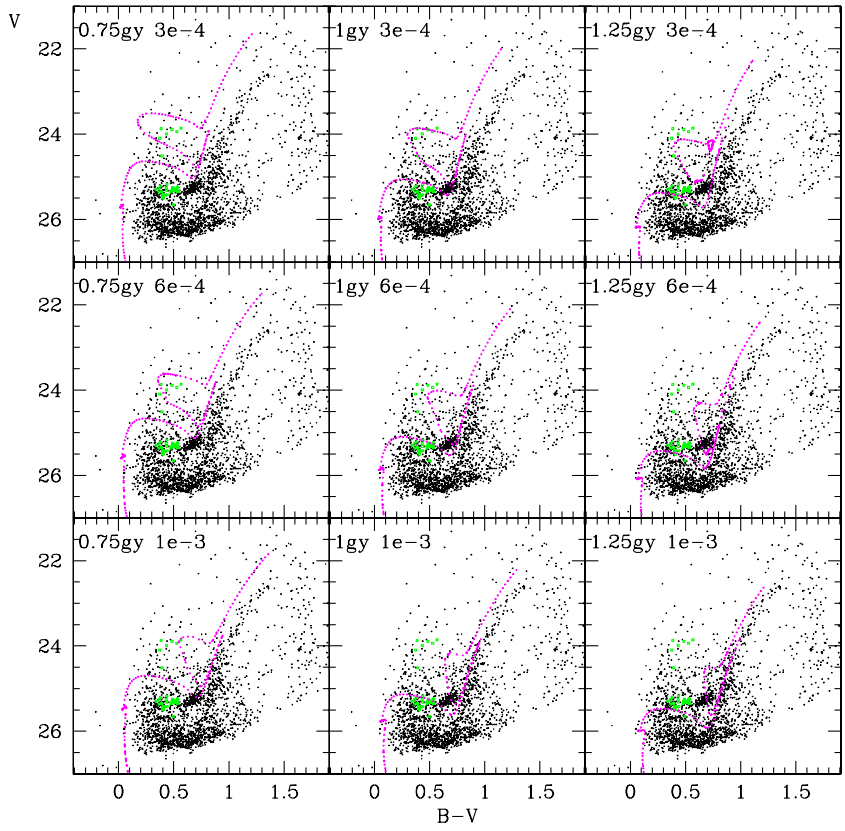

Figure 13. Same as Figure 10, but for metallicities from the top to the bottom panel of $Z = 0.0003$, 0.0006, and 0.001, respectively, and younger isochrones.
(A color version of this figure is available in the online journal.)

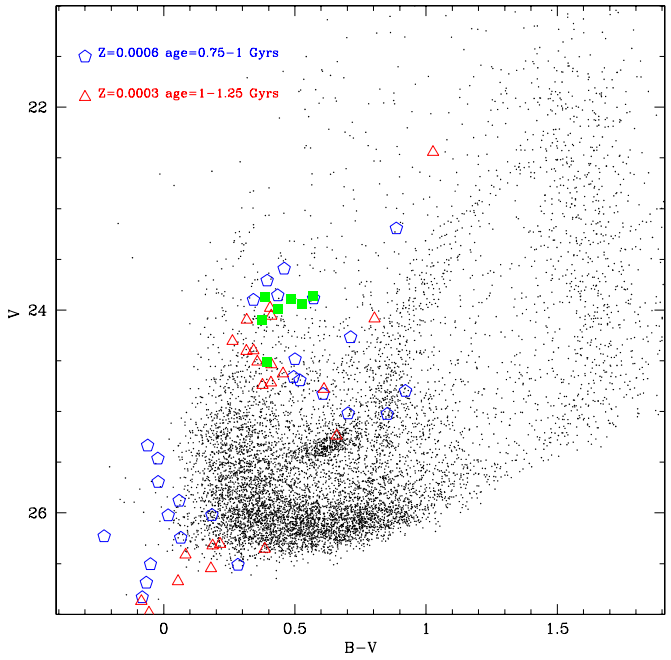

Figure 14. Synthetic stellar population allowing to reproduce the number of ACs (green squares) on the observed CMD (see Section 10.2 for details).
(A color version of this figure is available in the online journal.)

we used the Padova tracks (Marigo et al. 2008; Bertelli et al. 2009), convolved with photometric errors and incompleteness as estimated from artificial star tests and a Salpeter initial mass function. Once the number of synthetic objects populating the region 23.5 mag $< V <$ 24.5 mag and 0.2 mag $< B - V <$ 0.9 mag equaled the number of brighter pulsators, the procedure was stopped, giving the minimum amount of SF necessary to generate the brighter variables. This led to an SF rate of the order of $10^{-5}\,M_{\odot}$ yr^{-1}. Figure 14 shows the resulting simulations (blue pentagons and red triangles indicate $Z = 0.0006$ and $Z = 0.0003$ simulations, respectively) overlaid to the observed CMD. Although the exact CMD morphology of the ACs is not perfectly reproduced, both synthetic populations show a number of MS stars (objects at $V > 25.5$ mag), which is not much lower than star counts observed in the corresponding CMD regions. This suggests that if ACs are associated with a genuine SF episode, our inferred rate can be considered an upper limit to the recent activity in And XIX.

The other way of accommodating the apparent youth is that these stars are the evolved counterpart of MS blue stragglers. In this case, they are not the result of a recent episode of SF, but rather the result of mass transfer in close binary systems occurred about 1 Gyr ago. Unfortunately, the detection of MS blue stragglers or genuine young stars in the MS is greatly hindered by the contamination of blue galaxies.

11. SUMMARY AND CONCLUSIONS

We have presented B and V time-series observations of the M31 dSph satellite And XIX, which we performed using the LBC at the LBT. A total number of 39 variable stars were identified in the galaxy of which 31 are RR Lyrae stars and 8 are likely ACs. From the average period of the RRab stars and the period-amplitude diagram, we classify And XIX as an Oo-Int system. The average V magnitude of the RR Lyrae stars allowed us to estimate the distance modulus of And XIX, $(m - M)_0 = 24.52 \pm 0.23$ mag (for $E(B - V) = 0.11 \pm 0.06$ mag, as we derive from the RR Lyrae stars) or $(m-M)_0 = 24.66 \pm 0.17$ mag (for $E(B - V) = 0.066 \pm 0.026$ mag as derived from Schlegel et al. 1998 maps). Both estimates are in good agreement with the value of $(m - M)_0 = 24.57^{+0.08}_{-0.43}$ mag found by Conn et al. (2012). Comparing the observed CMD with stellar isochrones we find evidence for two different stellar populations in And XIX. One mostly made by old (13 Gyr) and metal poor ([Fe/H] $= -1.8$ dex) stars that produced the RR Lyrae variables, and the second composed by metal enriched stars ($-1.5 <$ [Fe/H] < -1.7 dex) with ages between 6 and 10 Gyr. The presence of ACs in And XIX provides hints for a recent episode of SF in this galaxy. With the use of evolutionary tracks and isochrones, we constrained this formation episode in an epoch between 0.75 and 1.25 Gyr ago. The ACs are found to follow well a PW relation and are mostly a genuine population belonging to And XIX with very little or no contamination by the M31 halo. The specific frequency of ACs in And XIX is also consistent with the value typical of other dSph galaxies in M31 and the MW. Finally, the spatial distribution of the RGB and HB stars gives an indication of the presence of a bar-like structure elongated in the direction of the M31 center.

We warmly thank P. Montegriffo for the development and maintenance of the GRATIS software; G. Beccari for useful suggestions on the estimate of the photometric completeness with ALLFRAME; and Flavio Fusi Pecci, Monica Tosi, and Carla Cacciari for useful comments and discussions on an earlier version of the paper. Financial support for this research was provided by COFIS ASI-INAF I/016/07/0 and by PRIN INAF 2010 (PI: G. Clementini). The LBT is an international collaboration among institutions in the United States, Italy, and Germany. LBT Corporation partners are The University of Arizona on behalf of the Arizona university system; Istituto Nazionale di Astrofisica, Italy; LBT Beteiligungsgesellschaft, Germany, representing the Max-Planck Society, the Astrophysical Institute Potsdam, and Heidelberg University; The Ohio State University; and The Research Corporation, on behalf of The University of Notre Dame, University of Minnesota, and University of Virginia. We acknowledge the support from the LBT-Italian Coordination Facility for the execution of observations, data distribution, and reduction.

Facility: LBT

REFERENCES

Abazajian, K. N., Adelman-McCarthy, J. K., Ageros, M. A., et al. 2009, ApJS, 182, 543
Bailey, S. I. 1902, AnHar, 38, 1
Barning, F. J. M. 1963, BAN, 17, 22
Bell, E. F., Slater, C. T., & Martin, N. F. 2011, ApJL, 742, L15
Bertelli, G., Nasi, E., Girardi, L., & Marigo, P. 2009, A&A, 508, 355
Bressan, A., Marigo, P., Girardi, et al. 2012, MNRAS, 427, 127
Brown, T. M., Ferguson, H. C., Smith, E., et al. 2004, AJ, 127, 2738
Cacciari, C., Corwin, T. M., & Carney, B. W. 2005, AJ, 129, 267
Carretta, E., Bragaglia, A., Gratton, R., D'Orazi, V., & Lucatello, S. 2009, A&A, 508, 695
Catelan, M. 2009, Ap&SS, 320, 261
Cignoni, M., & Tosi, M. 2010, AdAst, 2010, 158568
Clementini, G. 2010, in Variable Stars, the Galactic Halo and Galaxy Formation, ed. C. Sterken, N. Samus, & L. Szabados (Moscow: Sternberg Astronomical Institute of Moscow Univ.), 107
Clementini, G., Contreras Ramos, R., Federici, L., et al. 2009, ApJL, 704, L103
Clementini, G., Contreras Ramos, R., Federici, L., et al. 2011, ApJ, 743, 19
Clementini, G., Di Tomaso, S., Di Fabrizio, L., et al. 2000, AJ, 120, 2054
Clementini, G., Gratton, R., Bragaglia, et al. 2003, AJ, 125, 1309
Coe, D., Benitez, N., Sanchez, S. F., et al. 2006, AJ, 132, 926

Collins, M. L. M., Chapman, S. C., Rich, R. M., et al. 2013, ApJ, 768, 172
Conn, A. R., Ibata, R. A., Lewis, G. F., et al. 2012, ApJ, 758, 11
Contreras Ramos, R., Clementini, G., Federici, L., et al. 2013, ApJ, 765, 71
Federici, L., Cacciari, C., Bellazzini, M., et al. 2012, A&A, 544, 155
Gilbert, K. M., Guhathakurta, P., Beaton, R. L., et al. 2012, ApJ, 760, 76
Gratton, R. G., Bragaglia, A., Clementini, G., et al. 2004, A&A, 421, 937
Harris, W. E. 1996, AJ, 112, 1487
Ibata, R., Martin, N. F., Irwin, M., et al. 2007, ApJ, 671, 1591
Irwin, M. J., Ferguson, A. M. N., Huxor, A. P., et al. 2008, ApJL, 676, L17
Jeffery, E. J., Smith, E., Brown, T. M., et al. 2011, AJ, 141, 171
Lomb, N. R. 1976, Ap&SS, 39, 447
Mackey, A. D., Huxor, A. P., Martin, N. F., et al. 2013, ApJL, 770, L17
Madore, B. F. 1982, ApJ, 253, 575
Mancone, C., & Sarajedini, A. 2008, AJ, 136, 1913
Marconi, M., Fiorentino, G., & Caputo, F. 2004, A&A, 417, 1101
Marigo, P., Girardi, L., Bressan, et al. 2008, A&A, 482, 883
Martin, N. F., Ibata, R. A., Irwin, M. J., et al. 2006, MNRAS, 371, 1983
Martin, N. F., McConnachie, A. W., Irwin, et al. 2009, ApJ, 705, 758
Martin, N. F., Slater, C. T., Schlafly, E. F., Morganson, E., & Rix, H.-W. 2013, ApJ, 722, 15
Mateo, M., Fischer, P., & Krzeminski, W. 1995, AJ, 110, 2166
McConnachie, A. W. 2012, AJ, 144, 4
McConnachie, A. W., Huxor, A., Martin, N. F., et al. 2008, ApJ, 688, 1009
McConnachie, A. W., Irwin, M. J., Ibata, R. A., et al. 2009, Natur, 461, 66
Oosterhoff, P. T. 1939, Obs, 62, 104
Piersimoni, A. M., Bono, G., & Ripepi, V. 2002, AJ, 124, 1528
Pietrinferni, A., Cassisi, S., Salaris, M., & Castelli, F. 2004, ApJ, 612, 168
Piotto, G., King, I. R., Djorgovski, S. G., et al. 2002, A&A, 391, 945
Pritzl, B. J., Armandroff, T. E., Jacoby, G. H., & Da Costa, G. S. 2002, AJ, 124, 1464
Pritzl, B. J., Armandroff, T. E., Jacoby, G. H., & Da Costa, G. S. 2005, AJ, 129, 2232
Pritzl, B. J., Jacoby, G. H., & Da Costa, G. S. 2004, AJ, 127, 318
Richardson, J. C., Irwin, M. J., McConnachie, A. W., et al. 2011, ApJ, 732, 76
Ripepi, V., Marconi, M., Moretti, M. I., et al. 2013, MNRAS, submitted (arXiv:1310.5967)
Sarajedini, A., Mancone, C. L., Lauer, T. R., et al. 2009, AJ, 138, 184
Scargle, J. D. 1982, ApJ, 263, 835
Schlegel, D. J., Finkbeiner, D. P., & Davis, M. 1998, ApJ, 500, 525
Slater, C. T., Bell, E. F., & Martin, N. F. 2011, ApJL, 742, L14
Soszynski, I., Poleski, R., Udalski, A., et al. 2008, AcA, 58, 163
Soszynski, I., Udalski, A., Szymanski, M. K., et al. 2008, AcA, 58, 293
Starkenburg, E., Hill, V., Tolstoy, E., et al. 2010, A&A, 513, 34
Stetson, P. B. 1987, PASP, 99, 191
Stetson, P. B. 1992, JRASC, 86, 71
Stetson, P. B. 1994, PASP, 106, 250
van den Bergh, S. 1975, in Stars and Stellar Systems, Vol. 9, ed. A. R. Sandage, M. Sandage, & J. Kristian (Chicago, IL: Univ. Chicago Press), 509
van den Bergh, S. 1993, MNRAS, 262, 588
Wen, Z. L., & Han, J. L. 2013, in IAU Symp. 295, The Intriguing Life of Massive Galaxies, ed. D. Thomas, A. Pasquali, & I. Ferreras (Cambridge: Cambridge Univ. Press), 188
Yang, S.-C., & Sarajedini, A. 2012, MNRAS, 419, 1362
Zucker, D. B., Kniazev, A. Y., Bell, E. F., et al. 2004, ApJL, 612, L121
Zucker, D. B., Kniazev, A. Y., Martinez-Delgado, D., et al. 2007, ApJL, 659, L21